PAPER

Evolution of dopant-induced helium nanoplasmas

To cite this article: S R Krishnan *et al* 2012 *New J. Phys.* **14** 075016

View the article online for updates and enhancements.

Evolution of dopant-induced helium nanoplasmas

S R Krishnan[1]**, Ch Peltz**[2]**, L Fechner**[1]**, V Sharma**[1]**, M Kremer**[1]**,
B Fischer**[1]**, N Camus**[1]**, T Pfeifer**[1]**, J Jha**[3]**, M Krishnamurthy**[3]**,
C-D Schröter**[1]**, J Ullrich**[1,4]**, F Stienkemeier**[5]**, R Moshammer**[1]**,
Th Fennel**[2,6] **and M Mudrich**[5,6]

[1] Max-Planck-Institut für Kernphysik, 69117 Heidelberg, Germany
[2] Institute of Physics, University of Rostock, Universitätsplatz 3,
D-18051 Rostock, Germany
[3] Tata Institute of Fundamental Research, 1 Homi Bhabha road,
Mumbai 400 005, India
[4] Physikalisch-Technische Bundesanstalt, Bundesallee 100, D-38116
Braunschweig, Germany
[5] Physikalisches Institut, Universität Freiburg, 79104 Freiburg, Germany
E-mail: mudrich@physik.uni-freiburg.de and thomas.fennel@uni-rostock.de

Abstract. Two-component nanoplasmas generated by strong-field ionization of doped helium nanodroplets are studied in a pump–probe experiment using few-cycle laser pulses in combination with molecular dynamics simulations. High yields of helium ions and a pronounced resonance structure in the pump–probe transients which is droplet size dependent reveal the evolution of the dopant-induced helium nanoplasma with an active role for He shells in the ensuing dynamics. The pump–probe dynamics is interpreted in terms of strong inner ionization by the pump pulse and resonant heating by the probe pulse which controls the final charge states detected via the frustration of electron–ion recombination.

[6] Authors to whom any correspondence should be addressed.

IOP Institute of Physics ⬥DEUTSCHE PHYSIKALISCHE GESELLSCHAFT

Contents

1. Introduction

Nanoplasmas generated by intense femtosecond laser pulses are being actively investigated for gaining insights into the ultrafast dynamics of highly excited matter on the nanoscale, which features extraordinary characteristics. In particular, the peculiar property of laser-driven nanoplasmas of emitting highly energetic particles and radiation opens up opportunities for application as novel sources of radiation and for particle acceleration [1, 2]. Besides, the dynamics of multi-component nanoplasmas turns out to crucially impact the envisaged goal of realizing single-shot ultrafast diffraction imaging of large natural systems in the x-ray domain [3].

As a result of dedicated experiments as well as simulations, the behavior of single-component nanoplasmas in intense near-infrared fs laser pulses (10^{14}–10^{16} W cm^{-2}) is fairly well understood (see [1, 2] and references therein). These nanoplasmas are generated from neutral atomic aggregates or clusters via ionization by intense (IR) laser pulses. During this laser-driven ionization process, a large fraction of electrons released from their parent atoms or ions (inner ionization) remain trapped in the space charge field of the cluster [1, 2]. The optical response of the resulting nanoplasma is mainly determined by these quasi-free electrons. The most interesting properties of rare-gas clusters in the IR domain result from their high energy absorption per atom once ionized, by far exceeding the values achievable in atomic jets or planar solid targets [1, 2, 4]. A generic picture of the underlying dynamics can be built on the interrelation of the laser frequency ω_{las} and the time-dependent eigenfrequency ω_{res} of collective electronic dipole motion in the ionic background potential of the cluster. The dipolar eigenfrequency of the nanoplasma ω_{res} depends on the ionic charge density ρ, which for the spherical case is $\hbar\omega_{\text{res}} = \hbar\sqrt{e\rho/(3\varepsilon_0 m_e)}$ [1, 2]. Resonant driving conditions ($\omega_{\text{res}} = \omega_{\text{las}}$) are achieved on sub- or few-picosecond timescales when the plasma is diluted by ionic expansion. Furthermore, quasi-free electrons that gain sufficient kinetic energy within the laser–cluster interaction can escape the ionic potential of the nanoplasma, leading to 'outer ionization'.

In spite of this general understanding of the plasma dynamics, experiments have revealed surprises in the case of nanoplasmas from two- or multi-component clusters: intense IR pulse ionization of weakly doped ($<1\%$ doping) rare-gas clusters shows enhanced electron and characteristic x-ray yields as compared to their pristine counterparts under identical conditions [5, 6]. While in these cases the location of the dopant atoms could not be determined, extensive studies on the intense IR field ionization of metal and rare gas clusters embedded at the

centers of He nanodroplets have been carried out by the group of K-H Meiwes-Broer [2, 7–10]. These studies highlight the role of the embedded dopant kernel in the nanoplasma dynamics and ionic motion thereof.

As compared to free metal clusters, resonance conditions were found to be reached at earlier delay times when measuring the charge state spectra of the embedded species [7, 11]. The appearance of He^+ and He^{2+} ions in the latter was attributed to charge-transfer collision of highly charged metal ions in the kernel with the surrounding He atoms and was in agreement with the observed reduction in the maximum charge of the metal ions as compared to the free clusters. In large droplets, caging of ionization fragments was observed, which induces reaggregation and the formation of snowball complexes [7, 12].

The active role of the He droplet in plasma dynamics was initially discerned by numerical simulations [13–16]. From molecular dynamics (MD) studies it was concluded that the He shell undergoes rapid ionization and resonant heating following avalanche-like ionization of the dopant kernel [7, 16]. In a simplified picture, the distinct local ionic charge densities in the core containing dopant ions and in the surrounding He shell lead to two different dipolar eigenfrequencies (ω_{res}) of collective electron motion in the respective regions of the nanoplasma. As a consequence, during the expansion of this composite system, the driving laser field comes into resonance with the nanoplasma twice as a function of pump–probe delay. Thus, a double resonance is predicted to occur in the delay-dependent absorption and photo-electron spectra. The absence of a pronounced signature for such a double resonance in the pump–probe dependence of final ion charge spectra of the dopant ions was attributed to the complex interrelation of inner ionization and the subsequent recombination dynamics.

In this paper, we report a combined experimental and numerical study of the evolution of a dopant-induced He nanoplasma. It extends our recent experiments using single 10 fs pulses, which have demonstrated the ignition of He droplets induced by only a few dopant atoms [17]. Pump–probe measurements with identical 10 fs pulses carried out under the same experimental conditions together with the corresponding numerical simulations reveal a sensitive dependence of the optimal delays for the maximal yield of He ions on the size of the nanodroplet. Thus, the explicit role played by the ionized He atoms from the host matrix in the expansion dynamics of the composite nanoplasma is clearly established. We find good qualitative agreement between the experimental transient He ion yields and simulations of He charge states as a function of pump–probe delay when explicitly taking into account electron–ion recombination.

2. Experiment

He nanodroplets are an ideal host medium for designing well-defined nanometer-sized two-component clusters [18]. Owing to their weak coupling to dopant atoms and to their superfluid state, He droplets can pick up other rare gas atoms in a doping cell that aggregate to form clusters immersed in the droplet interior [18, 19]. The experimental arrangement is schematically shown in figure 1. A beam of He nanodroplets is produced by expanding pressurized ^{4}He gas (70–90 bar) through a nozzle 5 μm in diameter maintained at a temperature of 15–25 K. By varying the nozzle temperature in this range the mean number of He atoms per droplet is adjusted in the range 10^3–10^5. In a second vacuum chamber further downstream, the skimmed droplet beam passes through a 3 cm long cylindrical doping cell through two collinear apertures (∅ = 3 mm). A pressure gauge is directly attached to this cell for monitoring the local pressure. By leaking into the cell a controlled amount of krypton (Kr) or xenon (Xe) rare gas using
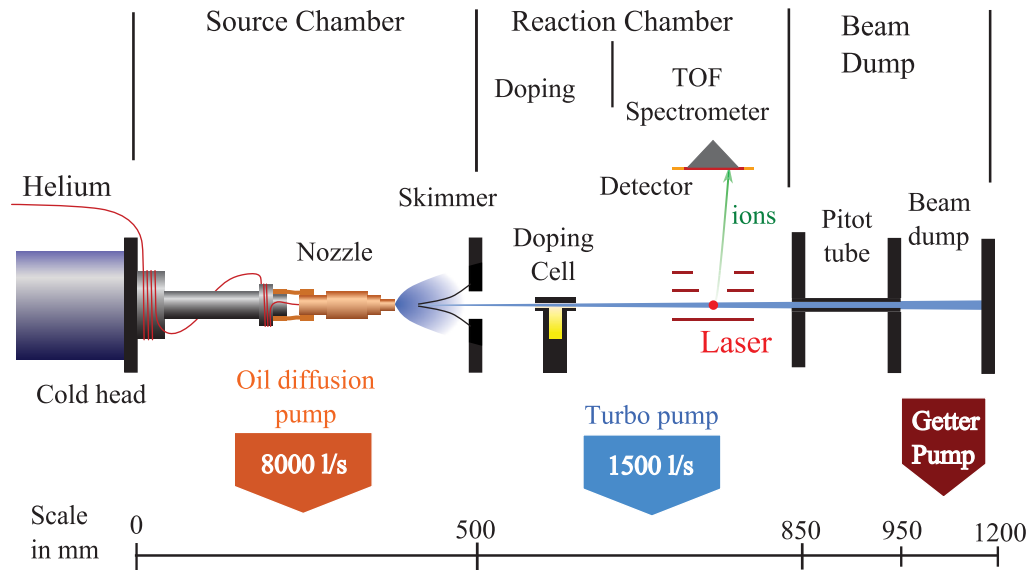
Figure 1. Experimental arrangement: schematic diagram of the assembly consisting of the He nanodroplet source, the doping chamber, the time-of-flight (TOF) spectrometer and the beam dump.

a dosing valve (leak rate $<10^{-10}$ mbar l s^{-1}) the mean number of dopants per nanodroplet K can be adjusted. Taking into account the shrinkage of He droplets due to evaporation of He atoms induced by the pick-up and cluster aggregation process, K can be determined from the cell pressure and the droplet size according to modified Poissonian pick-up statistics [20]. This model is validated using Monte-Carlo simulations of the pick-up process as detailed in [21].

Intense few-cycle laser pulses ($\sim$10 fs) at a central wavelength of 790 nm with peak intensities in the range of 10^{14}–10^{15} W cm^{-2} are generated by a Ti-sapphire-based mode-locked laser system (Femtopower, Femtolasers GmbH, Vienna). Pairs of identical pulses are created using a Mach–Zehnder interferometer. The delay time between the first 'pump' and the subsequent 'probe' pulse is adjusted by varying the length of one of the arms of the interferometer by moving a pair of retro-reflecting mirrors mounted on a piezo-driven translation stage. The collinearly aligned pump and probe pulses are focused by a spherical mirror (focal length $f = 100$ mm) into the beam of doped He nanodroplets. Photoions are detected by a time-of-flight (TOF) spectrometer in the Wiley–McLaren geometry. Since the characteristic timescale for changes of the optical response due to expansion of ionizing He nanodroplets is $\gtrsim 25$ fs [13, 16], the ultrashort pulses used in the present experiment ($\sim$10 fs) are well suited for probing the dynamics of such systems.

3. Theory

To model the intense laser–nanodroplet interaction, we employ a quasi-classical MD approach. Therein ions and plasma electrons are described classically and interact via their binary Coulomb forces. Atomic ionization events via tunneling and electron impact ionization (EII) are modeled quantum mechanically under the inclusion of the local plasma field resulting from plasma electrons and ions. Electron–ion recombination is taken into account for calculating ion

charge state distributions. The key aspects relevant to the present study are sketched briefly below; for a more detailed description of the numerical method, see [16, 22].

We consider as model systems He nanodroplets ($N_{\mathrm{He}} = 5000$, $10\,000$ and $15\,000$) doped with 20 Xe atoms. The nanodroplets are initialized as spheres (fcc structure) at the atomic density of liquid helium ($\rho = 0.022\,\text{Å}^{-3}$ [18]). After inserting the Xe_{20} core, He atoms with Xe neighbors closer than the equilibrium He–Xe distance of $4.15\,\text{Å}$ are removed [23]. All atoms in the doped nanodroplets are initialized in their charge neutral state. Electron liberation into the nanodroplet environment (inner ionization) via tunnel ionization (TI) and EII is described statistically via appropriate rates. The probability for TI is evaluated from the instantaneous Ammosov–Delone–Krainov rates [24], employing the local electric field, which is directly evaluated from the sum over all mutual Coulomb interactions and spatially smoothed over the respective ionic cell. A successful TI event results in a new plasma electron at the classical tunnel exit and an incremented charge state of the residual ion. To suppress artificial ionization resulting from large tunnel lengths, we clamp the tunnel distance to half the distance to the next ion. EII is evaluated from the Lotz cross-sections [25], taking into account local plasma field effects, such as the depression of in-medium ionization potentials [22]. After a successful EII event the charge state of the corresponding atom or ion is increased and a new plasma electron is generated on top of the atom or ion under the constraint of energy conservation. The resulting ions and electrons are then propagated classically in the laser field and under the influence of binary Coulomb interactions via

$$m_i \ddot{\mathbf{r}}_i = q_i e \mathbf{E}_{\mathrm{las}} - \nabla_{\mathbf{r}_i} \sum_{i \neq j} V_{ij}, \tag{1}$$

where m_i, $q_i e$ and $\mathbf{r}_i$ are the mass, charge and position of the ith particle and $\mathbf{E}_{\mathrm{las}}$ describes the laser electric field of two linearly polarized Gaussian laser pulses. The pairwise Coulomb interaction V_{ij} is described with a pseudopotential of the form

$$V_{ij}(r_{ij}, q_1, q_2) = \frac{e^2}{4\pi \varepsilon_0} \frac{q_i q_j}{r_{ij}} \, \mathrm{erf}\left(\frac{r_{ij}}{s}\right), \tag{2}$$

with the elementary charge e, the inter-particle distance r_{ij}, their charge states q_i and q_j and a numerical smoothing parameter s. The latter regularizes the Coulomb interaction and offers a simple route for avoiding classical recombination of electrons below the lowest possible quantum mechanical energy level. In our case, the smoothing parameter is determined by He and has a value of $s = 0.67\,\text{Å}$. The time-consuming evaluation of particle–particle interactions is accelerated using massive parallel computation techniques.

For the identification of resonance absorption in different regions of the doped droplet, we perform a spatially resolved analysis of the energy absorption from the laser field. To this end the droplet is divided into time-dependent spherical regions Ω_{core} and Ω_{shell}, which contain 95% of the Xe core atoms and the surrounding He droplet, respectively. The instantaneous power absorption in region Ω_k is determined from the dipole velocity by

$$P^{\Omega_k}(t) = \sum_{\mathbf{r}_i \in \Omega_k} e \, q_i \dot{\mathbf{r}}_i \cdot \mathbf{E}_{\mathrm{las}}(t), \tag{3}$$

leading to the accumulated energy absorption

$$W_{\mathrm{abs}}^{\Omega_k}(t) = \int_{-\infty}^{t} P^{\Omega_k}(t') \, \mathrm{d}t'. \tag{4}$$
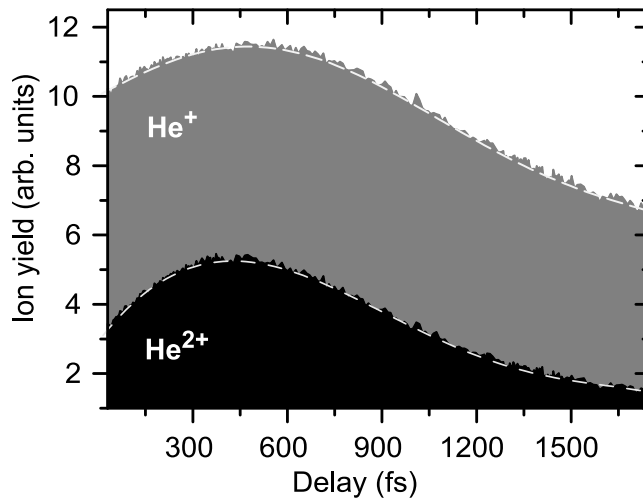
Figure 2. He^+ and He^{2+} ion yields as a function of pump–probe delay when He nanodroplets doped with Xe atoms are exposed to two identical pulses ($\sim 10\,fs$) of peak intensity $7 \times 10^{14}\,W\,cm^{-2}$. The mean droplet size is $15\,000$ He atoms, and the mean number of Xe dopants is 15 ± 3. The lines are a guide to the eyes.

For a meaningful comparison of the experimental and theoretical results, final ion charge spectra have to be determined from the simulation. Recent studies have shown that recombination has a crucial impact on the charge distributions and thus must be taken into account for predicting realistic charge spectra [15, 16, 22]. The two relevant mechanisms for recombination of quasi-free electrons with atomic ions after laser excitation are radiative recombination and three-body recombination (TBR). As has been estimated previously [22], radiative recombination can be neglected due to low rates [26]. TBR, i.e. electron capture after the collision of two quasi-free electrons in the vicinity of an ion, proceeds mainly to high Rydberg states of the ion and can therefore be treated classically. Hence, TBR is automatically included in reasonable approximation within the classical MD propagation. Besides the dominant contribution of TBR, even higher-order collisional recombination processes (four-body, five-body, etc) are accounted for because of the fully microscopic description of the effective classical particle–particle correlations. A key advantage of the direct microscopic treatment of recombination is that no approximations such as quasi-charge neutrality or a thermal electron velocity distribution need to be used. In addition, the local field effects due to screening and potentials of neighboring ions are included. To approximate the resulting charge spectra from the MD simulation, electrons are treated as recombined when bound to a specific ion after 1 ps of propagation subsequent to the probe pulse. For details see [16].

4. Results

4.1. Pump–probe dynamics

Figure 2 shows a typical example of He^+ and He^{2+} ion yields as a function of pump–probe delay measured with He droplets containing on average $15\,000$ He atoms doped on average by 15 ± 3 Xe atoms. Both ion signals exhibit a pronounced pump–probe dynamics on the sub-ps
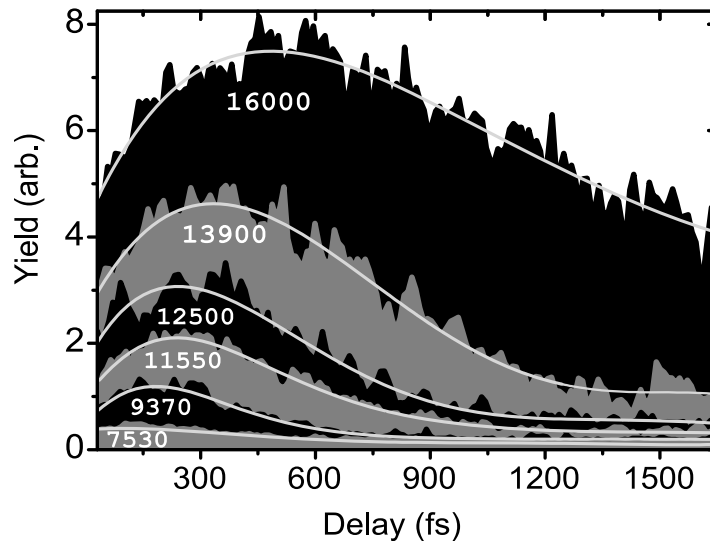
Figure 3. Experimentally measured delay dependence of He^{2+} ion yields for various droplet sizes in the range of 7500–16 000 He atoms per droplet (as indicated within the figure) for doping with 15 ± 3 Xe atoms. The peak intensity of the pump and probe pulses is 7×10^{14} W cm^{-2}. The curves are a fifth-order polynomial from which the optimal delay values (τ_{opt}) are extracted.

timescale with maximum yields of He^{2+} at $\tau_{opt} = 457$ (± 15) fs and of He^+ at $\tau_{opt} = 476$ (± 15) fs. Note that the He^{2+} signal shows higher pump–probe contrast and reaches a maximum at a slightly smaller value of the optical delay ($\Delta \tau_{opt} \approx 20$ fs).

In a simplified picture, the existence of an optimal delay can be interpreted as a signature of resonantly enhanced charging [7, 10, 16]. After the pump pulse ionizes the doped droplet and creates an overdense nanoplasma, the probe pulse excites the system resonantly after an appropriate degree of expansion. At the near-solid atomic densities prevalent within the droplet during the pump pulse, the dipolar eigenfrequency ($\hbar\omega_{res} \approx 3.2$ eV) by far exceeds the frequency $\hbar\omega_{las} \approx 1.6$ eV of the laser pulses at a wavelength of 790 nm under the assumption of homogeneous single ionization of the droplet. Hence, ionic expansion due to Coulombic and hydrodynamic forces is required to reach resonant conditions. As a consequence, the absorption of energy from the probe laser pulse by the ionized droplet rises sharply, leading to enhanced charging of the droplet nanoplasma and ion emission therefrom. A detailed analysis of the full pump–probe evolution of the nanoplasma is presented in the following section.

The delay dependence of the He ion yields is investigated for various experimental parameters. The He^+ and He^{2+} resonance curve shapes and peak positions turn out to be a robust feature with respect to variations of the laser pulse intensities as well as of the number and type of dopant atoms. Different rare gases (Ar, Kr, Xe) as well as molecular dopants (CO_2) have been used. The most pronounced peak shifting and broadening is observed when the size of the He droplets is varied. Figure 3 presents the delay dependence of He^{2+} ion yields for varying droplet size as indicated in the legend for the case of doping with ~15 Xe atoms. Clearly, the optimal delay τ_{opt} increases with increasing droplet size. This is similar to the delay dependence measurements of optical absorption by pure Xe clusters of different sizes observed by Zweiback *et al* [27] that were rationalized mainly by geometrical effects. Figures 4(a) and (b) illustrate the
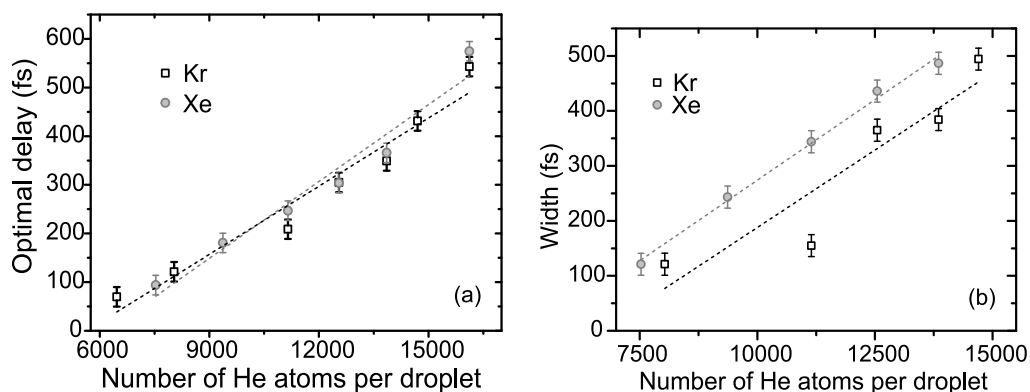
Figure 4. (a) Optimal delay times for doped He nanodroplets of various sizes. The corresponding variation of the widths (full-width at half-maximum (FWHM)) of ion yield curves is shown in panel (b). The mean number of doped Xe and Kr atoms is 15 ± 3 and 14 ± 3, respectively. The peak intensity of the pump and probe pulses is $7 \times 10^{14} \, \text{W cm}^{-2}$.

measured size dependences of the optimal delay and peak width (FWHM) as obtained by fitting the pump–probe data for Xe as well as Kr doping (figure 3) with a fifth-order polynomial. Both quantities are found to vary roughly linearly with the average number of He atoms per droplet in the considered size range.

4.2. Simulation results

In order to extract the mechanisms underlying the experimentally observed pump–probe dynamics we have performed MD simulations with doped He nanodroplets $Xe_{20}He_N$ exposed to two 10 fs pulses at the intensity $I = 7 \times 10^{14} \, \text{W cm}^{-2}$. Note that this intensity is well below the threshold for barrier suppression ionization of He, but sufficient for TI of Xe [28].

Figure 5 shows the time evolution of selected key observables for laser excitation of a $Xe_{20}He_{5000}$ droplet for two different pump–probe delays. The shorter delay is chosen such that resonant heating in the He droplet is induced by the second pulse (left panels), while the longer delay is not sufficient to excite any resonance (right panels). The simulations show that charging begins in the pump pulse with tunnel ionization of the dopant atoms residing at the droplet center. Laser heating of the first released electrons induces an impact ionization avalanche that quickly increases the charge states of the dopant core and the closest He shells around it. Subsequently, triggered by the plasma produced in the core region, the rest of the He nanodroplet becomes ionized from inside-out; see figures 5(a) and (e). As a result of ionization and heating during the pump pulse the droplet starts to expand (figures 5(c) and (g)). Due to the low atomic mass of He the shell explodes much faster than the core region and reaches the critical density for resonant excitation earlier, roughly 150 fs after the peak of the pump pulse. The corresponding critical radii for the expected shell and core resonance are indicated by blue and red circles in figures 5(c) and (g).

Using the estimated pulse delay for resonant heating ($\Delta t = 150 \, \text{fs}$), very efficient energy absorption in the He region can be observed (figure 5(b)). When compared to the absorption during the pump pulse, it is enhanced by a factor of 25, leading to significant direct
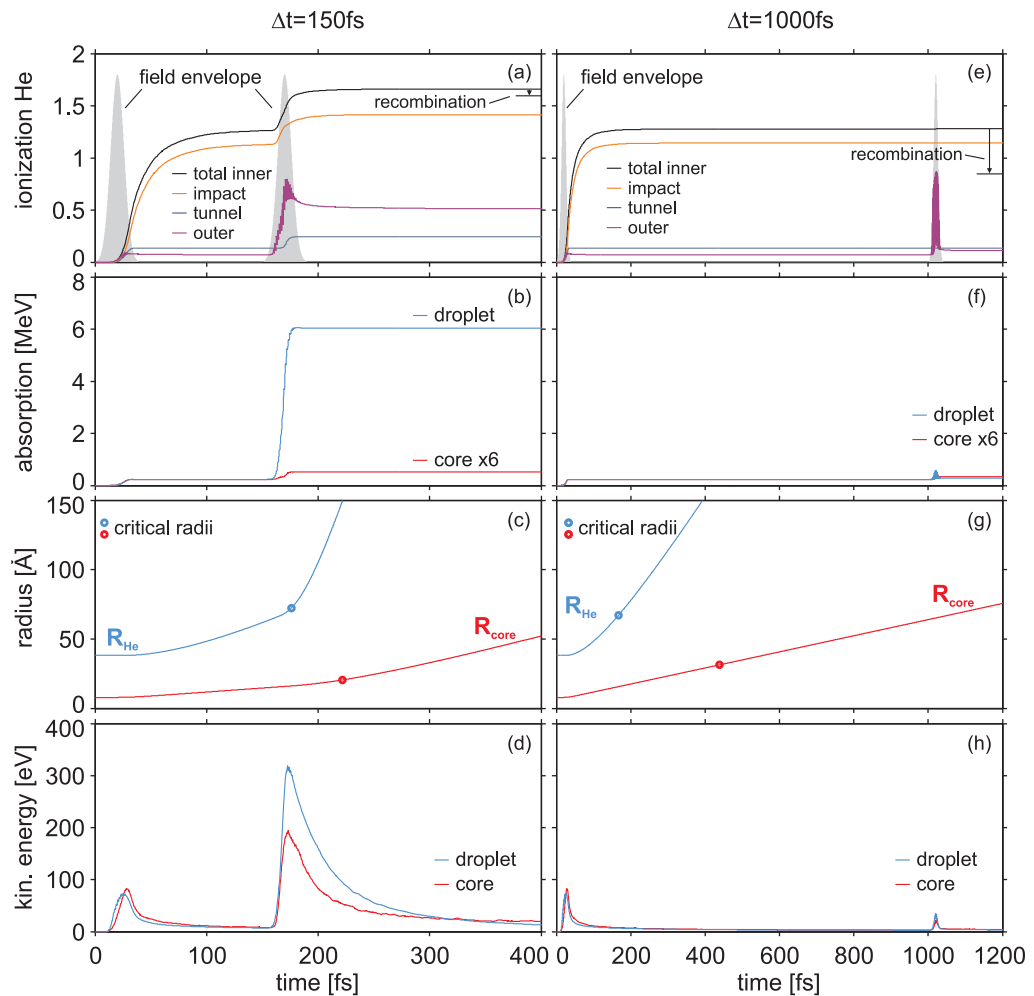
Figure 5. Calculated time evolution of the inner and outer ionizations, absorption, droplet and core radii (circles indicate estimated radii for resonant excitation) and average electron energy in the core and shell regions (top to bottom) for $Xe_{20}He_{5000}$ under two 10 fs laser pulses for a short ($\Delta t_1 = 150$ fs) and a long ($\Delta t_2 = 1000$ fs) delay at intensity $I = 7 \times 10^{14}$ W cm^{-2}.

outer ionization (figure 5(a)) and high electron temperatures (figure 5(d)). The absorption enhancement in the core region is much smaller, reflecting the still overcritical density in this region. As the core region is defined by a sphere containing 95% of the Xe atoms/ions, its boundary clearly separates the dopant and droplet species in the beginning of the simulation prior to any expansion. During subsequent expansion, the outermost Xe atoms start to overrun part of the He atoms due to their drift motion acquired in early stages of the interaction, where the nanoplasma is most strongly heated in the core region. However, the expansion speed and therewith the charge density of the core region are still governed by the expansion of the much heavier Xe ions. Coming back to the pump–probe dynamics, a much longer pulse delay (right panels) yields only very weak heating, weak outer ionization and small electron kinetic energies during the second pulse, reflecting a late stage of expansion with very low, undercritical nanoplasma densities.

For a realistic comparison of theory and experiment, charge spectra have to be determined by taking into account recombination processes. The resulting average He charge states calculated with our simplified recombination scheme are indicated by vertical arrows in figures 5(a) and (e). The effect of recombination is reflected by the difference between the average inner ionization and the final charge states. A comparison of the recombination efficiencies for both delays shows a strongly reduced recombination (less than 5%) for efficient nanoplasma heating at the short delay and much more efficient recombination (more than 30%) for the long, nonresonant delay. This trend reflects the strong temperature dependence of collisional recombination.

Figure 6 provides a systematic analysis of the pump–probe dynamics of absorption, ionization and recombination for three different droplet sizes, $N = 5000$, $10\,000$ and $15\,000$, from left to right. Focusing on the smallest nanodroplet first, the following general conclusions can be extracted (see the left panels in figure 6). The average inner charge state of He, i. e. the average number of electrons removed from He atoms, is significantly enhanced for short pulse delays. This reflects the density dependence of the inner ionization rates, as both the probability for electron–ion collisions as well as the influence of local plasma fields decrease with decreasing density. Note that no direct signature of resonant heating can be found in the pump–probe traces of inner ionization. In contrast to that, pronounced maxima occur in the energy absorption of the He nanodroplet (around 175 fs) and the absorption in the core region (around 450 fs); see figure 6(a). As a measure of outer ionization, the number of continuum electrons per He atom (purple curve in figure 6(d)) exhibits the same pump–probe delay dependence as the total energy absorption. The maxima in absorption and outer ionization clearly indicate resonant heating of the nanoplasma within the droplet.

In contrast to the inner charge state, the final charge state shows a strong delay dependence over the whole investigated range including a maximum for a delay of 150 fs and a shoulder near $\Delta t = 450$ fs; see figure 6(d). Again, the effect of recombination is reflected by the difference between the average inner ionization and the final charge states. Because of the high-temperature dependence of TBR, recombination is substantially suppressed in the case of enhanced heating of the nanoplasma. A comparison of the inner and the final charge states with the absorption in figure 6(a) shows that recombination is ineffective for delays with high absorption. This trend is most pronounced for resonant heating of the He shell. Furthermore, the resonant heating of the core region is also sufficient to significantly suppress recombination and leads to a shoulder in the final charge around 450 fs delay. The peak structure in the final charge states can be traced back to the combined action of inner ionization and resonant heating, in agreement with previous results [16].

A comparison of the results for different droplet sizes reveals the same trends, and shows that the above picture is generic for the pump–probe excitation of the doped nanodroplets and in reasonable agreement with the experimental findings. For all sizes of the He matrix, a pronounced peak in the final charge state is predicted. The peak values appear for delay times similar to the experiment and are shifted toward longer delays with increasing size of the He droplet. The increase of the optimal delays can be traced back to the fact that a larger matrix requires more time to expand to resonant conditions. Note that a quantitative comparison would require substantially larger numerical efforts to account for the experimental averaging over droplet and dopant cluster sizes as well as laser intensities [1, 2], which is beyond the scope of this work.
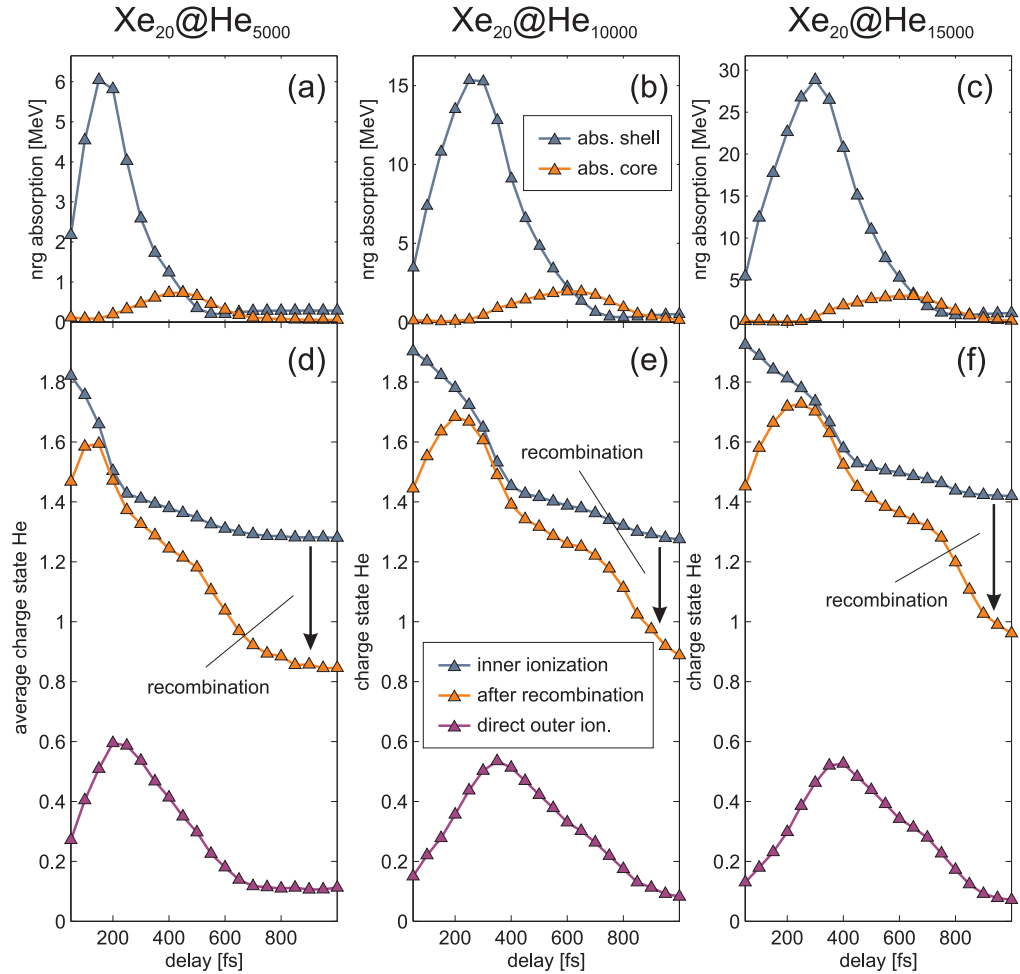
Figure 6. Calculated pump–probe dynamics of $Xe_{20}He_N$ after excitation with two 10 fs pulses (intensity: $I = 7 \times 10^{14}\,W\,cm^{-2}$) for three different droplet sizes, $N = 5000$, 10 000 and 15 000 from left to right. The upper panels (a)–(c) show the energy absorption in the He shell and in the Xe region (as indicated) as a function of pulse delay. In the bottom panels (d)–(f), average charge states for inner and outer ionization as well as final average charge states including recombination are given for different time delays.

5. Conclusions

We have studied the evolution of dopant-induced He nanoplasmas with a combination of experimental and classical MD simulations. High yields of He^+ and He^{2+} ions are experimentally observed when doping He nanodroplets with a few Kr or Xe atoms upon irradiation with pairs of few-cycle IR laser pulses. The He ion signals exhibit a pronounced resonance feature as a function of the pump–probe delay time, which most sensitively depends on the average size of the He droplets. A nearly linear increase in the optimal pump–probe delay as a function of the size of the nanodroplets clearly elucidates the dynamical role played by ionized He shells in the resonance of the composite nanoplasma. Our detailed numerical studies

IOP Institute of Physics ⚛ DEUTSCHE PHYSIKALISCHE GESELLSCHAFT

lead to the development of the following dynamical picture of the two-component nanoplasma evolution: (i) the whole interaction dynamics of the doped He nanodroplets is launched by TI of the dopant atoms. Heating of the first released electrons induces an impact ionization avalanche that charges up the whole droplet from inside to outside. (ii) The numerical calculations suggest that the varying recombination efficiency, which is minimal for resonant heating conditions, is a key mechanism behind the observed delay dependence of the charge states. (iii) The optimal delay for high ion yields depends most strongly on the droplet size. Therefore, the experimental data are the result of a convolution of the droplet size distribution as well as of the intensity profile of the laser focus. This leads to broader structures and masks details such as the numerically observed sideband due to the nanoplasma resonance at the core. Nevertheless, the salient features, i.e. the shift and the broadening of the observed resonance structures as a function of droplet size, are reproduced in the simulations.

The present studies motivate further experimental and theoretical investigations of the dynamics in two-component nanoclusters. While the present study brings to light the active role of the He shells in the nanoplasma expansion dynamics, it also opens up interesting questions for further investigation such as the effect of the location of the dopant atoms within the droplet (center versus surface) on the nanoplasma ionization and expansion dynamics.

Acknowledgments

References

[1] Saalmann U, Siedschlag Ch and Rost J M 2006 Mechanisms of cluster ionization in strong laser pulses. *J. Phys. B: At. Mol. Opt. Phys.* **39** R39
[2] Fennel Th, Meiwes-Broer K-H, Tiggesbäumker J, Reinhard P-G, Dinh P M and Suraud E 2010 Laser-driven nonlinear cluster dynamics *Rev. Mod. Phys.* **82** 1793–842
[3] Gaffney K J and Chapman H N 2007 Imaging atomic structure and dynamics with ultrafast x-ray scattering *Science* **316** 1444
[4] Ditmire T, Donnelly T, Rubenchik A M, Falcone R W and Perry M D 1996 Interaction of intense laser pulses with atomic clusters *Phys. Rev.* A **53** 3379–402
[5] Jha J and Krishnamurthy M 2008 Collisionless phenomena in heteronuclear clusters *Appl. Phys. Lett.* **92** 191108
[6] Jha J and Krishnamurthy M 2008 Hotter electron generation in doped clusters *J. Phys. B: At. Mol. Opt. Phys.* **41** 041002
[7] Döppner T, Diederich Th, Przystawik A, Truong N X, Fennel Th, Tiggesbäumker J and Meiwes-Broer K H 2007 Charging of metal clusters in helium droplets exposed to intense femtosecond laser pulses *Phys. Chem. Chem. Phys.* **9** 4639
[8] Döppner T, Fennel Th, Radcliffe P, Tiggesbäumker J and Meiwes-Broer K-H 2006 Ion and electron emission from silver nanoparticles in intense laser fields *Phys. Rev.* A **73** 031202
[9] Fennel Th, Döppner T, Passig J, Schaal C, Tiggesbäumker J and Meiwes-Broer K H 2007 Plasmon-enhanced electron acceleration in intense laser metal–cluster interactions *Phys. Rev. Lett.* **98** 143401

[10] Köller L, Schumacher M, Köhn J, Teuber S, Tiggesbäumker J and Meiwes-Broer K H 1999 Plasmon-enhanced multi-ionization of small metal clusters in strong femtosecond laser fields *Phys. Rev. Lett.* **82** 3783–6

[11] Döppner T, Teuber S, Diederich Th, Fennel Th, Radcliffe P, Tiggesbäumker J and Meiwes-Broer K H 2003 Dynamics of free and embedded lead clusters in intense laser fields *Eur. Phys. J.* D **24** 157–60

[12] Döppner T, Diederich Th, Göde S, Przystawik A, Tiggesbäumker J and Meiwes-Broer K-H 2007 Ion induced snowballs as a diagnostic tool to investigate the caging of metal clusters in large helium droplets *J. Chem. Phys.* **126** 244513

[13] Mikaberidze A, Saalmann U and Rost J M 2008 Energy absorption of xenon clusters in helium nanodroplets under strong laser pulses *Phys. Rev.* A **77** 041201

[14] Mikaberidze A, Saalmann U and Rost J M 2009 Laser-driven nanoplasmas in doped helium droplets: local ignition and anisotropic growth *Phys. Rev. Lett.* **102** 128102

[15] Döppner T, Müller J P, Przystawik A, Göde S, Tiggesbäumker J, Meiwes-Broer K H, Varin C, Ramunno L, Brabec T and Fennel Th 2010 Steplike intensity threshold behavior of extreme ionization in laser-driven xenon clusters *Phys. Rev. Lett.* **105** 53401

[16] Peltz C and Fennel Th 2010 Resonant charging of Xe clusters in helium nanodroplets under intense laser fields *Eur. Phys. J.* D **63** 281

[17] Krishnan S R *et al* 2011 Dopant-induced ignition of helium nanodroplets in intense few-cycle laser pulses *Phys. Rev. Lett.* **107** 173402

[18] Toennies J P and Vilesov A F 1998 Spectroscopy of atoms and molecules in liquid helium *Annu. Rev. Phys. Chem.* **49** 1

[19] Stienkemeier F and Lehmann K K 2006 Spectroscopy and dynamics in helium nanodroplets *J. Phys. B: At. Mol. Opt. Phys.* **39** R127

[20] Kuma S, Goto H, Slipchenko M N, Vilesov A F, Khramov A and Momose T 2007 Laser induced fluorescence of Mg-phthalocyanine in He droplets: evidence for fluxionality of large H_2 clusters at 0.38 K *J. Chem. Phys.* **127** 214301

[21] Bünermann O and Stienkemeier F 2011 Modeling the formation of alkali clusters attached to helium nanodroplets and the abundance of high-spin states *Eur. Phys. J.* D **61** 645–55

[22] Fennel Th, Ramunno L and Brabec T 2007 Highly charged ions from laser–cluster interactions: local-field-enhanced impact ionization and frustrated electron–ion recombination *Phys. Rev. Lett.* **99** 233401

[23] Chen C H, Siska P E and Lee Y T 1973 Intermolecular potentials from crossed beam differential elastic scattering measurements VIII. He + Ne, He + Ar, He + Kr and He + Xe *J. Chem. Phys.* **59** 601–10

[24] Ammosov M V, Delone N B and Krainov V P 1986 Tunnel ionization of complex atoms and of atomic ions in an alternating electromagnetic field *Sov. Phys.—JETP* **64** 1191–4

[25] Lotz W 1967 An empirical formula for the electron-impact ionization cross-section *Z. Phys.* A **206** 205–11

[26] Bethe H A and Salpeter E E 1977 *Quantum Mechanics of One- and Two-Electron Atoms* (New York: Plenum)

[27] Zweiback J, Ditmire T and Perry M D 1999 Femtosecond time-resolved studies of the dynamics of noble-gas cluster explosions *Phys. Rev.* A **59** R3166–9

[28] Augst S, Meyerhofer D D, Strickland D and Chint S L 1991 Laser ionization of noble gases by Coulomb-barrier suppression *J. Opt. Soc. Am.* B **8** 858–67